IEEE Access
Multidisciplinary ⋮ Rapid Review ⋮ Open Access Journal

Received November 8, 2019, accepted November 29, 2019, date of publication December 5, 2019, date of current version December 23, 2019.

Digital Object Identifier 10.1109/ACCESS.2019.2957857

Position Based Model of a Flexible Ureterorenoscope in a Virtual Reality Training Platform for a Minimally Invasive Surgical Robot

MARÍA PERAL-BOIZA[1], TERESA GÓMEZ-FERNÁNDEZ[1], PATRICIA SÁNCHEZ-GONZÁLEZ[1,2,3], BORJA RODRÍGUEZ-VILA[2,3,4], ENRIQUE J. GÓMEZ[1,2,3], (Senior Member, IEEE), AND ÁLVARO GUTIÉRREZ[1], (Senior Member, IEEE)

[1]E.T.S. Ingenieros de Telecomunicación, Universidad Politécnica de Madrid, 28040 Madrid, Spain
[2]Grupo de Bioingeniería y Telemedicina, E.T.S. Ingenieros de Telecomunicación, Centro de Tecnología Biomédica, 28040 Madrid, Spain
[3]Centro de Investigación Biomédica en Red de Bioingeniería, Biomateriales y Nanomedicina, 28029 Madrid, Spain
[4]Escuela de Arquitectura, Ingeniería y diseño, Universidad Europea de Madrid, 28670 Madrid, Spain

Corresponding author: Álvaro Gutiérrez (a.gutierrez@upm.es)

This work was supported by the ''Ministerio de Economía, Industria y Competitividad'' within the framework of the project ''LITHOS: Cirugía Robótica para el Tratamiento de Cálculos Renales'' under Grant RTC-2016-5338-1.

ABSTRACT Although the total number of ureteroscopy interventions during the past years has significantly increased, current flexible ureteroscopy procedures still present some limitations to urologic surgeons. However, nowadays different robotic systems have been developed in order to reduce those limitations. Flexible ureteroscopy robots provide a technological alternative which combines the benefits that this type of procedures offers to the patients, and solutions to the problems encountered from the surgeons perspective. In this paper, a virtual reality training platform for robot-assisted flexible ureterorenoscopy interventions is presented. A position based model for the virtual flexible endoscope is detailed and a standard user interface for the training platform is designed. Moreover, a comparative analysis of the performance of the training platform in different scenarios, including the navigation through a three-dimensional ureterorenal model, is presented. The obtained results determine that the training platform presents different computational rates depending on the complexity of the implemented environment and on the number of collisions and constraints that have to be handled. Nevertheless, the virtual model is visually plausible, effective for real-time user interaction and suitable for training.

INDEX TERMS Position based modelling, shape matching, flexible ureterorenoscopy, surgical simulation, training environment.

I. INTRODUCTION

The presence of calculi in the urinary tract is known as urinary lithiasis or urolithiasis. This urologic disease presents a high morbidity rate in the world. One out of 11 individuals suffers from kidney stones at some point in their lives, being the prevalence of stones equal to 8.8 % (10.6 % for men and 7.1 % for women) [1]. In addition, urolithiasis incidence in pediatric patients has significantly increased in the last decades [2], [3].

Urologic guidelines state since more than one decade that open stone surgery has to be considered only in exceptional situations, usually associated with calculi complexity, failure of previous minimally invasive interventions and patient anatomical abnormalities [4]. The renal and ureteral calculi treatment recommendations included in the recent European Association of Urology guidelines have changed towards endourologic procedures, such as ureteroscopy (URS) and

The associate editor coordinating the review of this manuscript and approving it for publication was Fabrizio Messina.

percutaneous nephrolithotomy (PNL), versus extracorporeal shockwave lithotripsy (SWL) [5]. Likewise, global urolithiasis treatment trends have clearly changed in the same direction, according to [6], that considered data of URS, PNL, SWL and open surgery interventions. The study also revealed the important uptrend in the use of URS technique and its promising future.

The incorporation of active tip deflection to passive flexible ureteroscopes represented an important advance in the exploration of the upper urinary tract by endourologic techniques. The deflection mechanism of the current flexible endoscopes includes one or two actively deflectable segments and a passive segment located proximal to the former. Whereas the active deflection of the tip is controlled by the surgeon with a mechanism on the handle of the endoscope, the passive deflection refers to the bending of the passive segment, which is more flexible than the rest of the endoscope, in contact with the urinary tract tissue [7]. The use of flexible ureteroscopy (fURS) has experienced determining improvements over the past years, including design modifications, miniaturization of the distal tip and deflection increase, along with new digital video technologies and intracorporeal lithotripsy devices [8]. These ongoing advances have led to an increase in the use of fURS and the expansion of its potential indications. It has been proved to be a safe and effective technique when performed with holmium laser lithotripsy in the treatment of urinary calculi, presenting high stone-free rate and low morbidity [9], [10].

However, although ureteroscopy techniques offer many benefits from the patient perspective, they also present some limitations to urologic surgeons. These surgical procedures involve serious ergonomics problems, as the surgeon maintains a standing position during the whole intervention, holding the ureteroscope up and turning the head to look at the endoscopy and fluoroscopy screens. This position leads to musculoskeletal pains and joints stiffness [11], [12]. Moreover, the endourologic surgeon is exposed to important doses of ionizing radiation from X-rays, used to acquire intraoperative images.

Nowadays, the objective of flexible ureteroscopy robots is to provide novel remotely controlled surgical systems, aiming for combining both the benefits that these procedures present for the patients and also solutions to the drawbacks they have from the surgeons point of view. These robotic systems are based on a robot for the endoscope manipulation located in the patient site, which is teleoperated by the surgeon from a control panel. This two-sites approach provides the urologic specialists with a more ergonomic workspace, remote from radiation sources.

A training environment that simulates a virtual reality platform of robot-assisted fURS has been developed. The objective of the implemented platform is to provide an effective training environment for urologic surgeons manipulating this type of robotic systems and to reduce the learning curve associated to the robotic system manipulation.

In a previous paper [13], the developed training platform, its user interface and general performance in different scenarios were presented and described. In this paper, the graphic algorithm implemented for the flexible endoscope virtual model is explained in detail in Section III. This algorithm is founded on the position based dynamics approach [14] and the shape matching method [15]. In Section IV, the results of the study and the comparative analysis of its performance in different scenarios are presented. These results are discussed in Section V. Finally, the conclusions drawn from this research and future lines of work are discussed in Section VI.

II. STATE OF THE ART

A. SURGICAL ROBOTS

Minimally invasive surgery (MIS) involves surgical procedures that aim to cause less damage to human tissue than traditional open surgical techniques. It is performed through small incisions or trocars, so its advantages over traditional open surgery are numerous: shorter recovering periods, minor postoperative complications, less scarring, shorter hospital stays, reduced pain and lower morbidity rate [16].

Moreover, MIS indications are widely expanded in many medical areas, like gynecology and urology [17], and it provides an effective and safe alternative to traditional open surgery in different types of surgical interventions [18]–[20]. In addition, advances in surgical instrumentation, focused on constant equipment miniaturization and refinement, have contributed to reduce tissue damage during MIS procedures.

However, MIS also presents several drawbacks. The learning curve for most surgeons is longer when compared to open surgery, and these procedures can also present longer operating time and higher equipment costs [21]. The occasional possibility of conversion to an open procedure due to intraoperative complications can occur during MIS interventions. A loss of the visibility of the operative area, the tactile perception and the surgeon dexterity are also associated with MIS. Moreover, ergonomics problems causing physical symptoms on surgeons have been repeatedly reported [22], [23].

Robot-assisted surgery is also becoming an expanded technology [24], [25]. Computer-assisted manipulation offers greater precision and can increase the surgeon dexterity during minimally invasive procedures [21]. Some of them also include haptic feedback, which intensifies enormously the immersive experience of the surgeon in the actual intervention. In addition, important ergonomic improvements from the surgeons point of view are achieved with robotic surgery systems when compared with traditional procedures [11], [12], [26], [27]. The feasibility of robotic-assisted minimally invasive procedures has been demonstrated in different types of interventions [28]–[30].

Currently available surgical robotic systems for minimally invasive procedures are performing interventions in different clinical areas, such as laparoscopy, catheterization and ureterorenoscopy. The Da Vinci surgical system (Intuitive Surgical Inc, CA, USA) is composed by four computer-manipulated robotic arms to operate the patient and a surgeon console provided with stereoscopic view, hand controls and pedals, where the specialist remains seated during the intervention. The robotic arms in the operative site system replicate identically the movements performed in the control console. It has been demonstrated to offer advantages over traditional MIS interventions [31], [32]. The TELELAP ALF-X surgical system (SOFAR S.p.A., ALF-X Surgical Robotics Department, Milan, Italy) provides a new robotic approach to minimally invasive procedures offering haptic feedback to the surgeon. It comprises a remote control unit with 3D vision and an eye-tracking camera control system. The patient site includes three or four manipulator arms. In contrast to the Da Vinci surgical system, it is not possible to use wristed instrumentation with the TELELAP ALF-X system, which is extremely useful in complex surgical interventions. Nevertheless, its feasibility and effectiveness in different clinical procedures have been reported [33]–[35]. The RAVEN Surgical Robot (University of Washington, WA, USA) is a robotic system for MIS procedures that provides haptic interaction. It includes the patient site with two articulated manipulators, and the surgeon site composed of two control devices and a video display from the operation field. The patient site is based on a spherical mechanism that has been optimized for the best kinematic performance of the system in a very compact workspace. It has been used in several telesurgical experiments, obtaining successful outcomes [36]. The robotic Percutaneous Access to the Kidney (PAKY) device (The Johns Hopkins Medical Institutions, MD, USA) is comprised of a radiolucent, sterilizable needle driver located at the terminal end of a robot arm. The movement of the needle is performed by a DC motor that is controlled with a joystick. It has been proved to be an effective and safe system in clinical interventions and in vitro experiments [37]. In addition, its accuracy and feasibility when combined with a remote center of motion (RCM) device have been determined in comparison to standard manual access [38]. The magnetic navigation system Niobe (Stereotaxis, MO, USA), for catheter interventions, is based on two computer-controlled permanent magnets that are located on opposite sides of the patient. They generate an external magnetic field that can be precisely manipulated in order to steer a small magnet in the distal tip of the catheter. The insertion of the catheter is controlled by a motor drive. Several clinical studies in patients determined the effectiveness of this system [39], [40]. The robotic catheter system Sensei X2 (Hansel Medical Inc, CA, USA) includes the remote catheter manipulator, the Artisan Extend Control Catheter and a remote surgeon console, with screens and a three-dimensional master controller device. The catheter tip replicates the movements performed on the console controller. The catheter system allows force feedback to the surgeon when performing surgical procedures. In addition, although this system was created for cardiac applications, it was demonstrated that the Sensei system is feasible for performing ureterorenoscopic interventions, after undergoing the required software and configuration modifications [41], [42]. Finally, the Avicenna Roboflex (ELMED, Ankara, Turkey) is a robot specifically designed for flexible ureteroscopy. It is composed of the surgeon console and the manipulator of the flexible endoscope. Two joysticks and pedals, a wheel and a control monitor allow manipulating the endoscope from the remote unit. The manipulator is composed of a motor system and a robotic arm where the endoscope is fixed. Moreover, a system in the robotic arm allows the insertion of the laser fibre for the lithotripsy procedure. It was reported to be a suitable and safe system in clinical interventions [11], [43].

Although many robotic surgical systems have been designed for MIS interventions, just a few of them are able to work on flexible ureteroscopy [44].

B. SURGICAL SIMULATION IN FLEXIBLE URETEROSCOPY

The benefits of surgical simulation in medical training, including robot-assisted surgery, have been repeatedly reported [45], [46]. Its advantages generally involve improvements in the efficiency and skills of the surgeon, learning curve reduction, improved educational experience, reduction in costs and easy access to different clinical scenarios. In addition, virtual reality (VR) simulation is becoming more widespread in medical applications. Several studies have already established the usefulness of VR simulation as a mean to train MIS technical skills [47].

Simulation platforms for ureterorenoscopy training have been previously developed [48], [49]. URO Mentor system (Simbionix, Tel Aviv, Israel) provides a platform for the simulation of rigid and flexible cystoscopic and ureterorenoscopic procedures. This platform allows training calculi lithotripsy and extraction, irrigation pressure control, contrast material injection and performing biopsies in real time simulation with realistic haptic feedback. It also provides anatomic and non-anatomic practice exercises with different levels of difficulty in order to acquire basic skills. It is composed of a personal computer and an operating table with a mannequin and a monitor for displaying intraoperative images [48]. The Scope Trainer (Mediskills Ltd., Edinburgh, United Kingdom) allows the user to simulate standard endoscopic procedures, such as flexible cytoscopy, rigid or flexible ureteroscopy or intracorporeal lithotripsy. This platform consists of a urinary tract model, including a distensible bladder, that can be accessed through the ureteral orifice in order to perform an endoscopic examination as in a real intervention. The Uro-Scopic Trainer (Limbs and Things, Bristol, United Kingdom) consists of a male genitourinary tract model that provides a training system for urethroscopy, cystoscopy, rigid and flexible ureteroscopy, lithotripsy and stone retrieval [50]. Similarly, the Adult Ureteroscopy Trainer (Ideal Anatomic Modelling, MI, USA) is a high-fidelity benchtop model of a collecting system. It is composed of the kidney, renal pelvis access, ureter and ureteral oriffice [51].

The surgical simulation platform presented in this paper is focused on the medical training for robot-assisted flexible ureterorenoscopy. It aims to reduce the learning curve associated to robotic system manipulation in a wide range of urolithiasis scenarios.

III. MATERIAL AND METHODS

The main objective of the implemented platform is to provide the urologists with a realistic and feasible environment for training for robot-assisted flexible ureterorenoscopy. This proposal will contribute to solve most of the ergonomic problems related to ureterorenoscopies that suffer the clinicians. As the main objective, it will move the clinicians from being in a stand up position with awkward head rotations and a lead vest during hours, to be sitting in a control console away from radiation. Therefore, the proposal follows a similar approach to the Da Vinci, TELELAP ALF-X or RAVEN Surgical Robots.

Diverse clinical cases can be simulated and presented to the surgeon, including different calculi locations and morphologies. The previous training aims to help them to acquire the required skills for performing ureteroscopy interventions with the robotic system and to reduce the learning curve. This environment can be also used for the surgical planning of future fURS interventions. The training platform presents a user interface identical to the one of the robotic system, in which the motions of the flexible ureteroscope are controlled remotely from the surgeon control panel and performed in the patient site by the final actuator system.

The development of the training platform was divided in two different phases: the design phase and the implementation phase. In the design phase, the requirements of the platform were defined and a very simple virtual model of the training environment was developed. This prototype was used to firstly evaluate the design of the final interface with specialists in ureterorenoscopy interventions. According to their feedback, separation between motions in different devices allows the surgeons to have a better control of the position of the endoscope distal tip. The implementation phase took the feedback provided by the surgeons as a starting point. In this phase, two 3D mice are used as endoscope controllers (see Figure 1). A 3D mouse is an electronic device that produces six degrees of freedom position and orientation information.

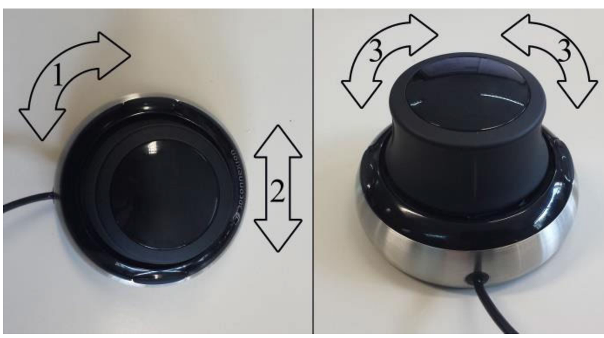

FIGURE 1. 3D mice used as endoscope controllers. (1) rotational, (2) insertion and (3) flexion motion.

The implemented flexible ureteroscope model has three degrees of freedom that are controllable by the surgeon: rotation, insertion and flexion. Rotation and insertion motions of the endoscope are manipulated with the left 3D mouse, whereas flexion motion is controlled with the right one. In addition, the developed training environment includes the simulation of intracorporeal lithotripsy procedure, calculi fragmentation monitoring and both intracorporeal views from endoscopy and fluoroscopy. The laser activation for lithotripsy is performed by pressing both side buttons of the right 3D mouse simultaneously, so as to minimize unintentional laser shots.

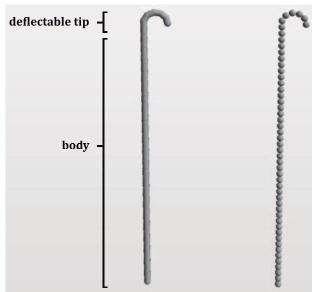

FIGURE 2. On the left, the continuous flexible endoscope model; on the right, its discretization.

In order to simulate the flexible endoscope, the solid model was discretized in a finite number of solid elements, as depicted in Figure 2. Being N the total number of nodes, each node is represented by the index i ($i \in [0, \ldots, N-1]$). The shape of the solid elements is spherical, defined by a specific radius, in order to simplify the implementation of the collision detection method. The flexible endoscope model developed is founded on the position based approach [14] and the shape matching method [15]. Vertical distance constraints, flexibility degree constraints and geometric constraints were established between the spherical nodes, as well as external collision constraints.

The three-dimensional endoscope model is divided into two sections which are modeled with different graphic algorithms: deflectable tip and body. The deflectable tip is based on the shape matching graphical approach. On the other side, the position based dynamics algorithm was used to model the performance of the endoscope body. The position of both sections is determined by the user input control over rotation, insertion and flexion levels, and also by the external collisions with environment objects. Moreover, it is important to point out that the positions of both sections are mutually dependent, since they actually constitute a solid body.

The control by the user of the three degrees of freedom of the endoscope impacts directly on the shape of the virtual model. Flexion motion actuates the endoscope tip, whereas endoscope insertion and rotation are performed from the insertion orifice and affect the whole model. However, since the rotation of the endoscope would only have a visual effect on the deflectable tip due to the spherical geometry of the solid nodes, it has been considered that rotational motion only actuates the endoscope tip for simplification.

A. INSERTION

As aforementioned, the simulation of the insertion movement is performed from the insertion orifice, in which the motion is originated and from where it propagates through the endoscope body. The position based dynamics method was implemented to model the body section [14]. This graphic approach is based on the modeling of virtual objects using directly positions instead of velocities, in contrast to traditional simulation methods. This approach aims to achieve stability and lower computational load with acceptable visual results.

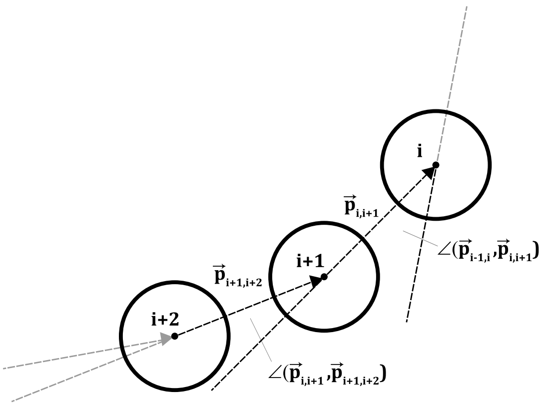

FIGURE 3. Section of the virtual endoscope body implemented: vertical distance constraints and flexibility degree constraints between adjacent nodes.

The algorithm consists of a solver iterator whose objective is to compute the scene solution that satisfies all the constraints of the points composing the virtual object. In order to fulfill this task, the constraints are repeatedly projected, i.e. the corresponding points of this constraint are relocated so as to satisfy the condition. The constraints that have been set in the virtual endoscope model are vertical distance constraints and flexibility degree constraints between adjacent nodes (see Figure 3), as well as external collision constraints. However, collision constraints generation and response are performed outside of the solver loop, as suggested in [14], obtaining satisfactory results.

Let $C(\vec{p})$ be an equality constraint function over the set of nodes positions $\vec{p} = \left[\vec{p}_0^T, \ldots, \vec{p}_n^T\right]^T$, $n \in [0, N-1]$. N is the total number of nodes that represent the virtual discretized model. This equality constraint function is satisfied if $C(\vec{p}) = 0$. In order to satisfy the constraint function $C(\vec{p})$, a correction $\Delta\vec{p}$ that makes $C(\vec{p} + \Delta\vec{p}) = 0$ must be found. This correction can be considered as the displacement of a node trying to satisfy the constraint function. This correction has to be in the direction of $\nabla_{\vec{p}} C(\vec{p})$ in order to achieve linear and angular momenta conservation if all the nodes have equal masses. This equation can be expressed as

$$C(\vec{p} + \Delta\vec{p}) \approx C(\vec{p}) + \nabla_{\vec{p}} C(\vec{p}) \cdot \Delta\vec{p} = 0 \tag{1}$$

$\Delta\vec{p}$ is calculated as

$$\Delta\vec{p} = \lambda \nabla_{\vec{p}} C(\vec{p}) \tag{2}$$

where λ is a scalar. By substituting Eq. 2 into Eq. 1, λ is calculated. Substituting it back into Eq. 2, the correction vector is obtained:

$$\Delta\vec{p} = -\frac{C(\vec{p})}{\left|\nabla_{\vec{p}} C(\vec{p})\right|^2} \nabla_{\vec{p}} C(\vec{p}) \tag{3}$$

The correction vector $\Delta\vec{p}_i$ for each node i involved in $C(\vec{p})$ is

$$\Delta\vec{p}_i = -s \nabla_{\vec{p}_i} C(\vec{p}) \tag{4}$$

where $s = \frac{C(\vec{p})}{\sum_h \left|\nabla_{\vec{p}_h} C(\vec{p})\right|^2}$ is the same for all nodes involved in $C(\vec{p})$.

If nodes with different masses m_i are considered, Eq. 2 can be expressed as

$$\Delta\vec{p}_i = \lambda\, w_i \nabla_{\vec{p}_i} C(\vec{p}) \tag{5}$$

with $w_i = 1/m_i$ and the correction vector $\Delta\vec{p}_i$ for each node i is

$$\Delta\vec{p}_i = -s\, w_i \nabla_{\vec{p}_i} C(\vec{p}) = -\frac{C(\vec{p})}{\sum_h w_h \left|\nabla_{\vec{p}_h} C(\vec{p})\right|^2} w_i \nabla_{\vec{p}_i} C(\vec{p}) \tag{6}$$

For every time step of the simulation, a fixed set of constraint functions is established. It is comprised by vertical distance constraints ${C_D}^j(\vec{p}^j)$ ($j \in [N_T - 1, \ldots, N_B - 2]$) and flexibility degree constraints ${C_F}^k(\vec{p}^k)$ ($k \in [N_T - 1, \ldots, N_B - 3]$), being N_B the number of nodes composing the body and N_T the number of nodes composing the deflectable tip of the endoscope virtual model. Moreover, a special degree constraint for the joint between the endoscope body and tip was set, $C_J(\vec{p}^J)$ ($\vec{p}^J = \left[\vec{p}_{N_T-2}, \vec{p}_{N_T-1}, \vec{p}_{N_T}\right]$). At each time step, the corrections of nodes positions involved in each constraint function ($\Delta\vec{p}_i^j$, $\Delta\vec{p}_i^k$ and $\Delta\vec{p}_i^J$) are calculated in a solver iterator which tries to satisfy all the established constraints.

The vertical distance constraint function is

$${C_D}^j(\vec{p}^j) = {C_D}^j(\vec{p}_i^j, \vec{p}_{i+1}^j) = {C_D}^j(\vec{p}_j, \vec{p}_{j+1}) = \left|\vec{p}_{j,j+1}\right| - d \tag{7}$$

being $\vec{p}_{j,j+1} = \vec{p}_j - \vec{p}_{j+1}$ and d the distance between the nodes with which the constraint is satisfied (see Figure 4). The solver iterator projects the constraints from the insertion point of the examined model to the endoscope tip inside the model. It was considered that the nodes outside of the examined model have infinite mass, since all of them have a fixed position controlled by the surgeon.

The gradients with respect to the node positions involved in the constraint are calculated as

$$\nabla_{\vec{p}_j} {C_D}^j(\vec{p}^j) = \frac{\vec{p}_j - \vec{p}_{j+1}}{\left|\vec{p}_{j,j+1}\right|} \tag{8}$$

$$\nabla_{\vec{p}_{j+1}} {C_D}^j(\vec{p}^j) = -\frac{\vec{p}_j - \vec{p}_{j+1}}{\left|\vec{p}_{j,j+1}\right|} \tag{9}$$

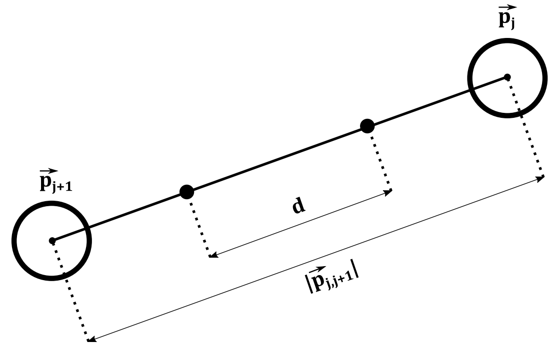

FIGURE 4. Geometric representation of the vertical distance constraint.

The scaling factor for ${C_D}^j(\vec{p}^j)$ is ${s_D}^j = \frac{|\vec{p}_{j,\,j+1}|-d}{w_j+w_{j+1}}$. Thus, the correction vectors are

$$\Delta\vec{p}_j = -\frac{w_j}{w_j + w_{j+1}}(|\vec{p}_{j,\,j+1}| - d)\frac{\vec{p}_{j,\,j+1}}{|\vec{p}_{j,\,j+1}|} \tag{10}$$

$$\Delta\vec{p}_{j+1} = +\frac{w_{j+1}}{w_j + w_{j+1}}(|\vec{p}_{j,\,j+1}| - d)\frac{\vec{p}_{j,\,j+1}}{|\vec{p}_{j,\,j+1}|} \tag{11}$$

The flexibility degree constraint function is

$$\begin{aligned} {C_F}^k(\vec{p}^k) &= {C_F}^k(\vec{p}^k_i, \vec{p}^k_{i+1}, \vec{p}^k_{i+2}) = {C_F}^k(\vec{p}_k, \vec{p}_{k+1}, \vec{p}_{k+2}) \\ &= \underline{\measuredangle(\vec{p}_{k,\,k+1}, \vec{p}_{k+1,\,k+2})} - \delta \end{aligned} \tag{12}$$

being $\vec{p}_{k,\,k+1} = \vec{p}_k - \vec{p}_{k+1}$ and $\vec{p}_{k+1,\,k+2} = \vec{p}_{k+1} - \vec{p}_{k+2}$ (see Figure 5). δ represents the angle between the vectors with which the constraint is satisfied.

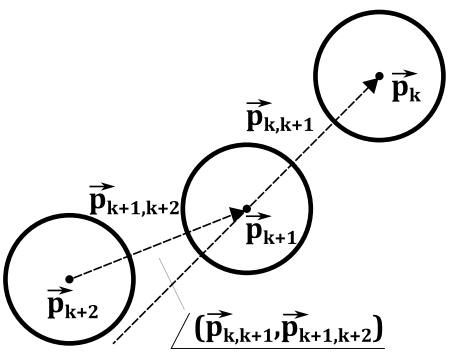

FIGURE 5. Geometric representation of the flexibility degree constraint.

This constraint function can be expressed as

$$\begin{aligned} {C_F}^k(\vec{p}_k, \vec{p}_{k+1}, \vec{p}_{k+2}) &= \vec{p}_{k,\,k+1} \cdot \vec{p}_{k+1,\,k+2} \\ &\quad - |\vec{p}_{k,\,k+1}|\,|\vec{p}_{k+1,\,k+2}| \cos\delta \end{aligned} \tag{13}$$

where the operator $(\cdot)$ represents the dot product of both vectors. As considered in the vertical distance constraint, the solver iterator projects the constraints from the insertion point to the endoscope tip. Moreover, the nodes outside of the examined model are considered to have infinite mass. The gradients with respect to the node positions involved in the constraint are calculated as

$$\nabla_{\vec{p}_k}{C_F}^k(\vec{p}^k) = \vec{p}_{k+1,\,k+2} - \vec{p}_{k,\,k+1}\frac{|\vec{p}_{k+1,\,k+2}|}{|\vec{p}_{k,\,k+1}|}\cos\delta \tag{14}$$

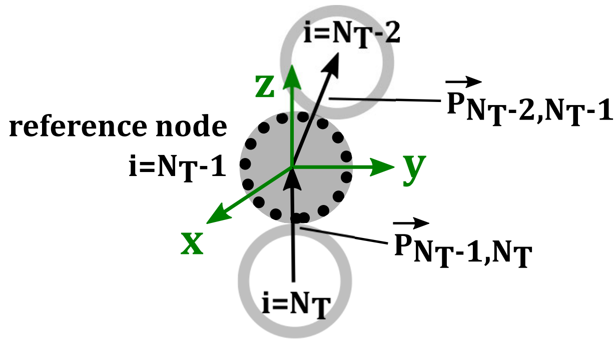

FIGURE 6. Geometric representation of the junction constraint.

$$\begin{aligned} \nabla_{\vec{p}_{k+1}}{C_F}^k(\vec{p}^k) &= \vec{p}_k - 2\vec{p}_{k+1} + \vec{p}_{k+2} \\ &\quad + \vec{p}_{k,\,k+1}\frac{|\vec{p}_{k+1,\,k+2}|}{|\vec{p}_{k,\,k+1}|}\cos\delta \\ &\quad - \vec{p}_{k+1,\,k+2}\frac{|\vec{p}_{k,\,k+1}|}{|\vec{p}_{k+1,\,k+2}|}\cos\delta \end{aligned} \tag{15}$$

$$\nabla_{\vec{p}_{k+2}}{C_F}^k(\vec{p}^k) = -\vec{p}_{k,\,k+1} + \vec{p}_{k+1,\,k+2}\frac{|\vec{p}_{k,\,k+1}|}{|\vec{p}_{k+1,\,k+2}|}\cos\delta \tag{16}$$

The scaling factor for ${C_F}^k(\vec{p}^k)$ is denoted by

$${s_F}^k = \frac{\vec{p}_{k,\,k+1} \cdot \vec{p}_{k+1,\,k+2} - |\vec{p}_{k,\,k+1}|\,|\vec{p}_{k+1,\,k+2}|\cos\delta}{L} \tag{17}$$

where

$$\begin{aligned} L = w_k\left|\nabla_{\vec{p}_k}{C_F}^k(\vec{p}^k)\right|^2 + w_{k+1}\left|\nabla_{\vec{p}_{k+1}}{C_F}^k(\vec{p}^k)\right|^2 \\ + w_{k+2}\left|\nabla_{\vec{p}_{k+2}}{C_F}^k(\vec{p}^k)\right|^2 \end{aligned} \tag{18}$$

Thus, the correction vectors are

$$\Delta\vec{p}_k = -{s_F}^k\, w_k \nabla_{\vec{p}_k}{C_F}^k(\vec{p}^k) \tag{19}$$

$$\Delta\vec{p}_{k+1} = -{s_F}^k\, w_{k+1} \nabla_{\vec{p}_{k+1}}{C_F}^k(\vec{p}^k) \tag{20}$$

$$\Delta\vec{p}_{k+2} = -{s_F}^k\, w_{k+2} \nabla_{\vec{p}_{k+2}}{C_F}^k(\vec{p}^k) \tag{21}$$

The special degree constraint function for the joint between the endoscope body and the deflectable tip is

$$\begin{aligned} C_J(\vec{p}^J) &= C_J(\vec{p}_{N_T-2}, \vec{p}_{N_T-1}, \vec{p}_{N_T}) \\ &= \underline{\measuredangle(\vec{p}_{N_T-2,\,N_T-1} \times \vec{p}_{N_T-1,\,N_T}, R_{1x})} - 0^\circ \end{aligned} \tag{22}$$

being $\vec{p}_{N_T-2,\,N_T-1} = \vec{p}_{N_T-2} - \vec{p}_{N_T-1}$ and $\vec{p}_{N_T-1,\,N_T} = \vec{p}_{N_T-1} - \vec{p}_{N_T}$. The operator $(\times)$ represents the cross product of two vectors.

This constraint function can be expressed as

$$\begin{aligned} &C_J(\vec{p}_{N_T-2}, \vec{p}_{N_T-1}, \vec{p}_{N_T}) \\ &\quad = (\vec{p}_{N_T-2,\,N_T-1} \times \vec{p}_{N_T-1,\,N_T}) \cdot R_{1x} \\ &\quad = (\vec{p}_{N_T-2,\,N_T-1} \times \vec{p}_{N_T-1,\,N_T}) \cdot R_{1x} \\ &\qquad - |\vec{p}_{N_T-2,\,N_T-1}|\,|\vec{p}_{N_T-1,\,N_T}| \sin(\delta_{ideal}) \end{aligned} \tag{23}$$

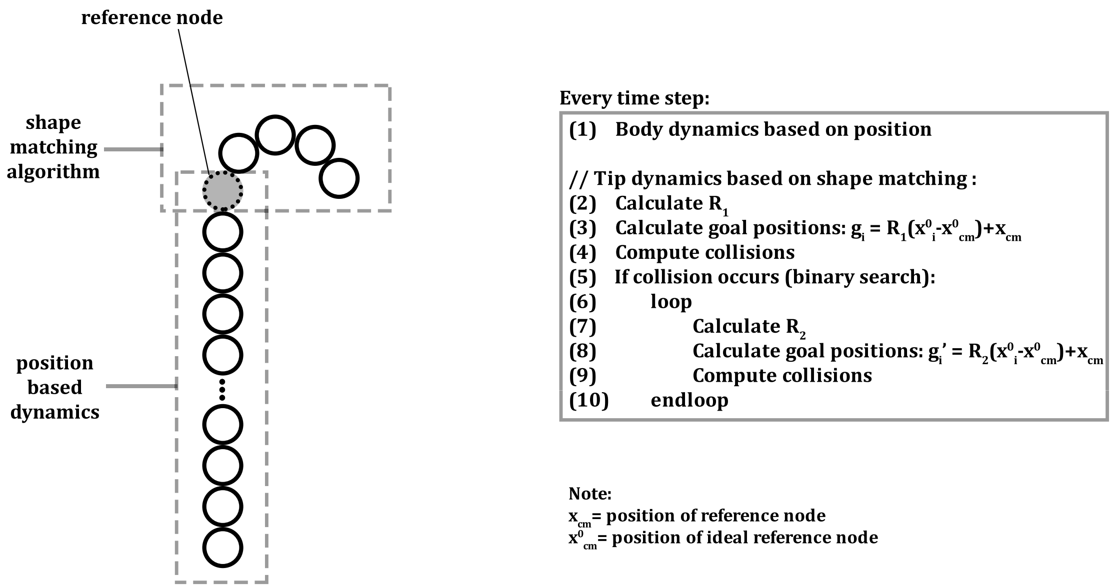

FIGURE 7. Simplified scheme followed for the flexion and rotation graphical computation.

where the operator $(\cdot)$ represents the dot product of both vectors, and δ_{ideal} is the angle between the corresponding vectors in the ideal shape of the endoscope tip without colliding. The geometric notion behind this constraint function is that the angle between vectors $\vec{p}_{N_T-2,\,N_T-1}$ and $\vec{p}_{N_T-1,\,N_T}$ has to be the angle between the ideal nodes vectors, calculated in the shape matching algorithm (see Section III-B). Moreover, the vector resulting from the cross product between vectors $\vec{p}_{N_T-2,\,N_T-1}$ and $\vec{p}_{N_T-1,\,N_T}$ has to be parallel to the x axis of the local reference frame of the so-called reference node $(i = N_T - 1)$ (see Figure 6). The rotation of this local reference frame is represented by the rotation matrix R_1 calculated in the shape matching algorithm.

Analogously to the previous cases, the gradients with respect to the node positions, $\nabla_{\vec{p}_{N_T-2}} C_J(\vec{p}^{\,J})$, $\nabla_{\vec{p}_{N_T-1}} C_J(\vec{p}^{\,J})$ and $\nabla_{\vec{p}_{N_T}} C_J(\vec{p}^{\,J})$, the scaling factor s_J and the correction vectors, $\Delta\vec{p}_{N_T-2}$, $\Delta\vec{p}_{N_T-1}$ and $\Delta\vec{p}_{N_T}$, are calculated. In this constraint case, the node in the endoscope tip $(i = N_T - 2)$ is considered to have infinite mass so that the shape matching algorithm remains unaltered. This junction constraint between the endoscope body and the tip provides position feedback from the tip to the body when a collision in the deflectable tip occurs.

Once the projected positions $\vec{p}_i$ have been calculated, the integration scheme implemented was the following

$$\vec{v}_i = \frac{\vec{p}_i - \vec{x}_i}{\Delta t} \tag{24}$$

$$\vec{x}_i = \vec{p}_i \tag{25}$$

where $\vec{v}_i$ is the velocity of the i-th node and $\vec{x}_i$ is the final position of the i-th node after the current time step.

B. FLEXION AND ROTATION

Both flexion and rotation actuate the deflectable section of the endoscope tip. The is modeled using a shape matching algorithm [15]. At every time step, the tip nodes try to reach previously computed goal positions $\vec{g}_i$ $(i \in [0, \ldots, N_T - 1]$, being N_T the number of nodes composing the deflectable tip of the endoscope virtual model). The goal positions are calculated as

$$\vec{g}_i = R(\vec{x}_i^{\,0} - \vec{x}_{cm}^{\,0}) + \vec{x}_{cm} \tag{26}$$

where $\vec{x}_i^{\,0}$ are the nodes positions of the ideal shape tip, $\vec{x}_{cm}^{\,0}$ is the center of mass of the ideal shape tip, $\vec{x}_{cm}$ refers to the center of mass of the actual shape, and R is a 3×3 rotation matrix that has to be computed every time step.

In order to efficiently calculate the goal positions $\vec{g}_i$ at every time step, the scheme depicted in Figure 7 is followed. The so-called reference node $(i = N_T - 1)$ is considered to have infinite mass and acts like a reference for locating the remaining tip nodes, whose masses are finite. The position of the reference node is previously determined by the position based dynamics algorithm, since it is also considered as part of the endoscope body. This method ensures that the tip will always be attached to the flexible body. Thus, the center of mass of the actual shape $\vec{x}_{cm}$ can be considered as the reference node position $(\vec{x}_{cm} = \vec{x}_{N_T-1})$. Likewise, the center of mass of the ideal shape $\vec{x}_{cm}^{\,0}$ is the position of the ideal reference node $(\vec{x}_{cm}^{\,0} = \vec{x}_{N_T-1}^{\,0})$. The rotation matrix R_1 represents the local rotation of the reference node. The rotation matrix R_2 is computed when penetration of the deflectable tip into external objects occurs.

In order to compute the rotation matrix R_2, external collisions of the endoscope tip with environment objects are taken into account. When the tip penetrates an external object at a time step, the developed algorithm recursively iterates to find a final position where the tip nodes are located inside the object surface, maintaining the endoscope tip shape. This algorithm is based on a balanced binary search tree paradigm, in order to reduce the number of iterations (see Figure 8).

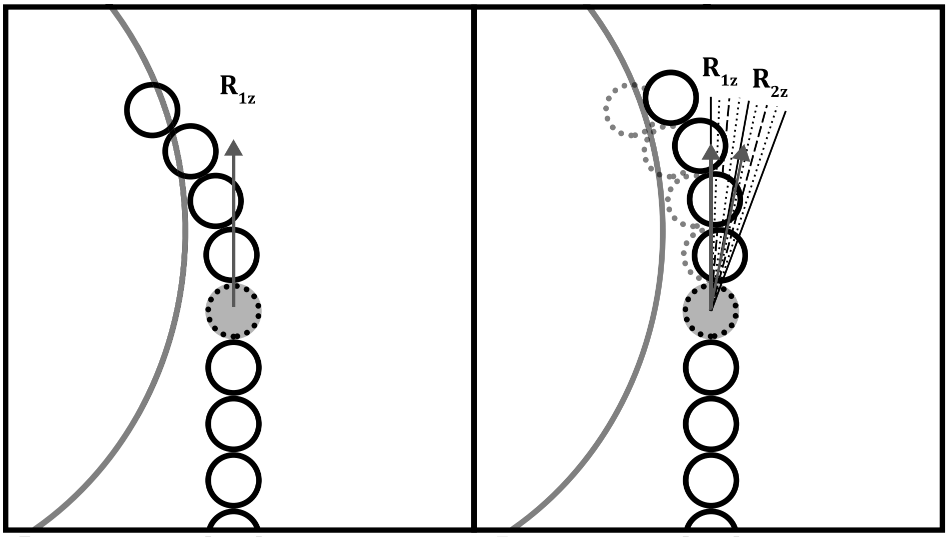

FIGURE 8. Simplified example of the implemented algorithm based on a binary search principle to compute the rotation matrix R_2, with a balanced binary tree of four levels.

The algorithm minimizes the distance between the penetrating tip position and the final tip position, preserving the initial shape of the tip at the current time step.

The ideal nodes positions $\vec{x}_i^0$ are calculated by applying forward kinematics of the flexible ureteroscope tip [52]. The model considers a discretized endoscope. The position $\vec{x}_i^0 (i \in [0, \ldots, N_T - 2])$ of the ideal node i can be calculated as

$$\vec{x}_i^0 = \begin{bmatrix} \vec{x}_{ref}^0.x \\ \vec{x}_{ref}^0.y + R(1 - \cos(\alpha - i\beta)) \\ \vec{x}_{ref}^0.z + R\sin(\alpha - i\beta) \end{bmatrix} \tag{27}$$

where $\beta = \frac{\alpha}{N_T - 1}$, $R = \frac{L}{\alpha}$, N_T is the number of nodes composing the virtual endoscope tip, α the flexion degree ($0 < \alpha < 270$), L the length of the distal tip and $\vec{x}_{ref}^0$ the known position of the ideal reference node ($\vec{x}_{ref}^0 = \vec{x}_{N_T - 1}^0$).

The ideal nodes positions $\vec{x}_i^0$ are recomputed every time the flexion degree of the endoscope tip (α) is reconfigured by the user interaction.

Once the goal positions $\vec{g}_i$ have been calculated, the integration method implemented was the following modified Euler scheme

$$\vec{v}_i(t + \Delta t) = \vec{v}_i(t) + \gamma \frac{\vec{g}_i(t) - \vec{x}_i(t)}{\Delta t} \tag{28}$$

$$\vec{x}_i(t + \Delta t) = \vec{x}_i(t) + \Delta t \vec{v}_i(t + \Delta t) \tag{29}$$

where $\vec{v}_i$ is the velocity of the i-th node, $\vec{x}_i$ is the position of the i-th node and γ is a parameter which simulates the stiffness of the object ($0 \leq \gamma \leq 1$). The higher value of γ, the higher stiffness the object presents.

C. SIMULATION ALGORITHM IMPLEMENTATION

The virtual system was developed using the C++ simulation framework CHAI3D [53], an open-source and multiplatform environment designed to integrate tactile and visual sensations in real time. It uses the OpenGL framework for 3D graphic rendering. CHAI3D includes several libraries for computer haptics, visualization and interactive real-time simulation, which make it a very useful platform for developing the integration of the implemented virtual environment with force feedback.

As shown in Figure 9, the basic architecture is composed of two different periodic tasks: the computational loop and the graphic rendering loop. The computational task has to calculate, at every time step, the final positions of the nodes of the virtual flexible ureteroscope and capture the user interaction inputs. The graphic rendering task has the objective of updating the visual scene.

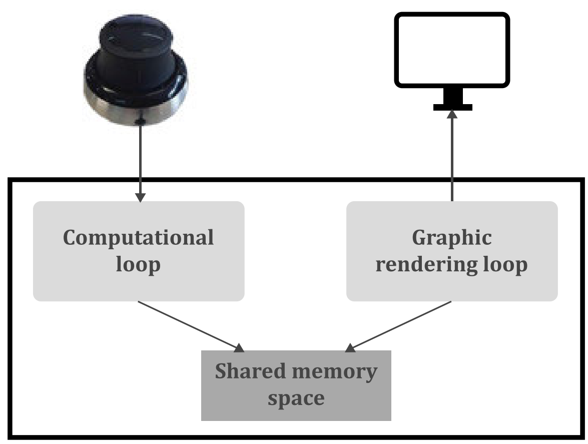

FIGURE 9. Basic architecture of the developed simulation program.

Both tasks are handled by two POSIX threads with different priorities. The computational loop is assigned the highest priority, because the execution of this task, which involves

FIGURE 10. Performance of the simulated endoscope model in three different scenarios (from left to right: Scenario 1, 2 and 3, respectively).

user interaction, requires the highest possible frequency. On the other side, the graphic rendering loop is assigned a lower priority. The minimum frequency required for this graphic update is 25 fps.

The collision detection method implemented provided by the CHAI3D framework is based on an axis-aligned bounding box hierarchy, in which virtual objects are wrapped in boxes aligned with the global coordinate system axes. In this approach, objects are organized creating a hierarchical tree topology. That is, small objects are wrapped in different bounding boxes and then in larger bounding volumes that contain other wrapped objects. With this method, the complexity of the detection algorithm may be reduced.

Regarding the collision response method, the force rendering approach "finger-proxy" of the CHAI3D framework was applied to the implemented graphic algorithm [54]. This force model is based on the idea of a virtual proxy that represents the real cursor movements towards a goal. This virtual proxy presents the same behaviour as a real pointer would have in real life; while haptic exploration, it does not penetrate external objects and lies on their surface during collisions. In free space, both proxy and goal positions are the same. When an external object avoids proxy direct motion to the goal, the algorithm tries to reduce the distance between the two points, moving the proxy along the object external surfaces until it reaches a position with the lower distance to the goal possible. Although the computational cost of this algorithm is higher than other alternative methods, like the potential field model, it solves some limitations like discontinuities in the object surface or pop-through of thin objects. The use of this complex force model may be beneficial in a future work for the integration of haptic feedback in the training platform.

IV. TEST AND RESULTS

In order to test the performance of the simulated flexible endoscope, different static tridimensional scenarios were created. These scenarios were composed of pipeline shaped

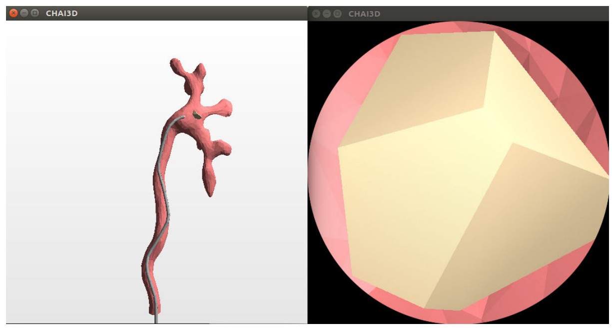

FIGURE 11. Implemented virtual reality environment user interface, including endoscopy (right) and fluoroscopy (left) screens.

objects with different configurations in which the endoscope can be inserted and advance. Figure 10 shows the response of the endoscope model implemented in three scenarios (Scenarios 1, 2 and 3) with non-anatomic appearance. Scenario 1 allows the system to test independent turns and Scenario 2 provides two concatenated turns. In both scenarios, only the insertion movement will allow the ureterorenoscope tip to reach the end of the pipeline, but colliding with the walls. However, users should not collide with the walls using flexion and rotation movements. Scenario 3 creates two clock-wise turns in a U-shape figure which obliges to have a good maneuverability with the ureterorenoscope. In this case, a simple insertion movement does not allow to reach the end of the pipeline, and flexion and rotation movements are mandatory. In the three scenarios, the training implies to reach the end of the pipeline.

In addition, navigation through a three-dimensional ureterorenal model was implemented (Scenario 4) for creating an accurate and realistic training platform. The 3D model was previously acquired with a CT scan on a real urinary tract. The developed training platform provides two different views: the endoscope monitor displaying real time intraoperative images and a remote view of the patient body equivalently to the fluoroscopic acquisition (see Figure 11). The equivalent X-rays view is only updated when required by the surgeon and allows the specialist to know the current exact location of the endoscope. In this Scenario, the training implies to reach the urinary calculi on the fluoroscopy screen (see Figure 11-right).

Usability tests were performed with 10 clinicians who did not have any previous contact with the training platform. The objective of validating the simulation and the behavior of the virtual ureterorenoscope was explained. They were instructed about the movement of the 3D mouse and how insertion, rotation and flexion were implemented. Two different flexion behaviors were tested: manual and automatic flexion. In automatic flexion, the ureterorenoscope tip goes back to the straight direction once the 3D mouse is released, as a real ureterorenoscope behaves. In the manual flexion, the ureterorenoscope tip keeps its position when the 3D mouse is released, as it occurs with insertion and rotation. Every surgeon tested the system siting in front of the screen with the 3D mice in between (see Figure 12). Objectives were achieved by all clinicians in the time provided for the platform testing.

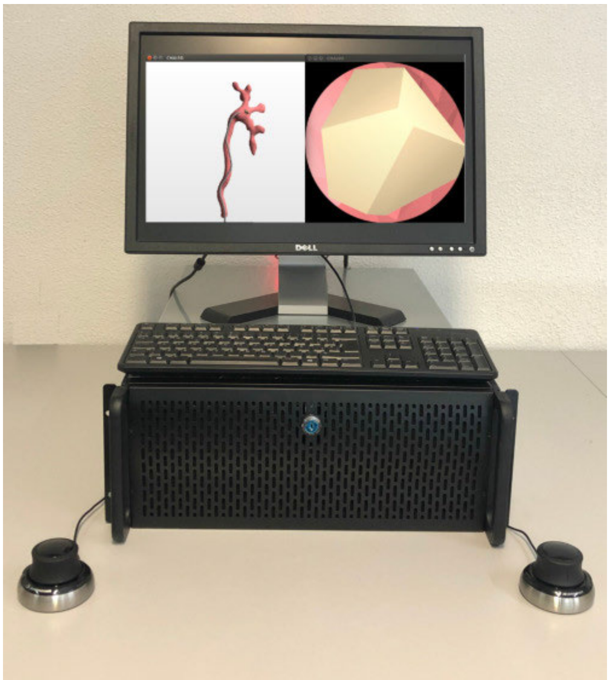

FIGURE 12. Complete system, with the screen and the two 3D mice.

A. COMPUTATION TEST

The frequency of the computational loop was measured in all experiments. The results obtained are presented in the Table 1. The number of spherical nodes comprising the virtual endoscope was 37.

As it can be seen in Table 1, the computational loop frequency is higher than 3 kHz in 90.7 % of the cases and lower than 1 kHz in 0.97 % of the cases.

TABLE 1. Comparison mean percentage of execution time running at the different frequency ranges in Scenarios 1, 2, 3 and 4.

	% of computational rate (Hz)						
Scenario	< 500	500–1000	1000–1500	1500–2000	2000–2500	2500–3000	> 3000
1	0.312	0.294	0.19	0.246	0.669	0.754	97.536
2	0.337	0.26	0.218	0.604	1.289	1.483	95.809
3	0.521	0.52	1.208	2.392	2.094	1.513	91.752
4	0.475	0.496	2.432	2.815	1.698	1.415	90.67

B. USABILITY TEST

A test based on the Likert scale was conducted to check the platform usability. Questions and anonymous answers, together with the mean and standard deviation are provided in Table 2. In general, the usability is very well scored: 4.40 for insertion, 4.70 for rotation and 4.10 for manual flexion. However, automatic flexion was not so well scored, 3.00 in average. The reason for this score is that, despite being the common behavior of a real ureterorenoscope, it is not very intuitive compared to the other 2 degrees of freedom. Moreover, clinicians stated that to keep the ureterorenoscope tip in its place by maintaining the 3D mouse in a specific position is not very common in any automated system. Therefore, manual flexion is the option preferred by all clinicians. Despite this punctualization, the platform as a whole is scored in average with 4.6 about is usage and 4.40 for its utility for robotic surgical training. Clinicians declared that the 3D mouse maneuverability is very adequate for training the usage of a robotic platform (4.40 out of 5.00 in average). Although it would require a learning curve for real operations, they emphasized that the 3D mouse is a very valid control device. Moreover, they found it comfortable and its integration into their clinical daily work would be favorable. Finally, they also noted that it could be very suitable for other procedures such as the treatment of tumors in the bladder or prostatic hyperplasias.

V. DISCUSSION

Regarding the obtained outcomes, it was determined that the most time-consuming task is the collision detection and handling, that is executed when the virtual endoscope model reaches a position in which the nodes are colliding with a complex obstacle and the constraints are not satisfied. Regarding the time intervals longer than 2 ms (frequencies lower than 500 Hz), it could be observed that they do not cause a detectable visual impact. Nevertheless, further studies must be undertaken in order to determine if they can pose a problem in the case that haptic feedback integration is implemented in the training platform.

The performance of the algorithm in the four scenarios is similar. However, lower frequencies are reached more often in the fourth environment. This behavior is expected as the geometry of the ureterorenal model is more complex than that of the other environments, leading to a higher number of collisions and constraints that have to be handled.

TABLE 2. Validation results of the 10 clinicians who tested the platform. Responses are based on a Likert scale, where 1 means strongly disagree and 5 means strongly agree. Average and standard deviations are provided for all questions.

	Clinician										Average	Std.
Question	1	2	3	4	5	6	7	8	9	10		
Q1: I found the insertion easy to use.	4	5	4	5	5	4	4	5	4	4	4.40	0.52
Q2: I found the rotation easy to use.	5	5	5	5	5	4	4	5	4	5	4.70	0.48
Q3: I found the manual flexion easy to use.	3	4	4	4	5	4	4	5	4	4	4.10	0.57
Q4: I found the automatic flexion easy to use.	1	3	2	4	4	4	4	2	4	2	3.00	1.15
Q5: The platform is globally easy to use.	4	4	4	5	5	5	4	5	5	5	4.60	0.52
Q6: The platform is of utility for robotic surgical training. i	4	5	5	5	5	5	2	5	4	4	4.40	0.97
Q6: The manipulation of the 3D mouse is adequate.	4	5	5	4	5	4	5	4	4	4	4.40	0.52

From the usability perspective, clinicians provided a very good impression and usability of the platform. All 3D movements sequences were very well accepted but the automatic flexion. Therefore, it must be improved in future implementations. Moreover, the platform has confirmed that the implementation of a real robotic system will solve most of the ergonomic problems present in ureterorenoscope surgeries. Clinicians will move from a standing position with awkward head positions during hours, to be sitting in a control console handling the tools from the 3D mice in good ergonomic positions. Nonetheless, further tests must be performed with an extensive number of clinicians and more real training tasks, such as Scenario 4.

VI. CONCLUSION AND FUTURE WORK

Flexible ureteroscopy robots provide a novel system that allows the remote control of the flexible endoscope by the use of robotics as an alternative to traditional ureterorenoscopy interventions. The main objective of the implementation of these robotic surgical systems is to meet the needs of both patients and surgeons, offering a solution to the limitations associated to the conventional fURS from the urologists point of view.

In this paper, a virtual training platform for robot-assisted ureterorenoscopy systems has been presented. It comprises the same interface of the robotic system, including the endoscope controllers, endoscopic and fluoroscopic screens and laser activation for lithotripsy procedures. First, the model implemented for the virtual flexible endoscope was explained in detail. After that, several experiments undertaken in order to analyze its performance in different scenarios, including the navigation through a three-dimensional ureterorenal model, were proposed. The obtained results determine that the training platform presents different computational rate depending on the complexity of the implemented environment and on the number of collisions and constraints that have to be handled. However, in this initial study it could be observed that this does not have any detectable visual impact.

The developed virtual environment offers a suitable tool for training urologic surgeons manipulating robotic systems in flexible ureterorenoscopy interventions. Usability tests with clinicians have increase the expectations of the virtual platform and its associated robotic platform. Clinicians find the proposal configuration with the two 3D mice and a screen where to have the endoscopy and fluoroscopy images very correct and comfortable. Moreover, it has been detected that the console configuration of two 3D mice could be very suitable for other surgery procedures.

Finally, future work is focused on the integration of the training platform with a force feedback system, in order to increase the immersion of the urologist in the actual surgical intervention. Future studies have to be performed so as to determine if the computational performance of the model developed is suitable for the combination with haptic feedback. In addition, a clinical validation has to be undertaken in order to determine the reduction of the learning curve of the surgeons in this type of interventions. Moreover, the development of dynamic environments may be appropriate to test the implemented training platform in a more accurate scenario. These realistic environments may include deformable tissue.

ACKNOWLEDGMENT

The authors acknowledge support for Robotics Special Applications S.L., Vicomtech-IK4 and the Instituto de Investigación Sanitario Biodonostia.

REFERENCES

[1] C. D. Scales, A. C. Smith, J. M. Hanley, C. S. Saigal, and Urologic Diseases in America Project, "Prevalence of kidney stones in the United States," *Eur. Urol.*, vol. 62, no. 1, pp. 160–165, 2012.

[2] J. C. Routh, D. A. Graham, and C. P. Nelson, "Epidemiological trends in pediatric urolithiasis at United States freestanding pediatric hospitals," *J. Urol.*, vol. 184, no. 3, pp. 1100–1105, 2010.

[3] D. J. Sas, T. C. Hulsey, I. F. Shatat, and J. K. Orak, "Increasing incidence of kidney stones in children evaluated in the emergency department," *J. Pediatrics*, vol. 157, no. 1, pp. 132–137, 2010.

[4] G. Alivizatos and A. Skolarikos, "Is there still a role for open surgery in the management of renal stones?" *Current Opinion Urol.*, vol. 16, no. 2, pp. 106–111, 2006.

[5] C. Türk, A. Petřík, K. Sarica, C. Seitz, A. Skolarikos, M. Straub, and T. Knoll, "Eau guidelines on interventional treatment for urolithiasis," *Eur. Urol.*, vol. 69, no. 3, pp. 475–482, 2016.

[6] R. Geraghty, P. Jones, and B. K. Somani, "Worldwide trends of urinary stone disease treatment over the last two decades: A systematic review," *J. Endourol.*, vol. 31, no. 6, pp. 547–556, 2017.

[7] J. B. Basillote, D. I. Lee, L. Eichel, and R. V. Clayman, "Ureteroscopes: Flexible, rigid, and semirigid," *Urologic Clinics North Amer.*, vol. 31, no. 1, pp. 21–32, 2004.
[8] D. T. Beiko and J. D. Denstedt, "Advances in ureterorenoscopy," *Urologic Clinics North Amer.*, vol. 34, no. 3, pp. 397–408, 2007.
[9] A. Breda, O. Ogunyemi, J. T. Leppert, J. S. Lam, and P. G. Schulam, "Flexible ureteroscopy and laser lithotripsy for single intrarenal stones 2 CM or greater—Is this the new frontier?" *J. Urol.*, vol. 179, no. 3, pp. 981–984, 2008.
[10] A. Breda, O. Ogunyemi, J. T. Leppert, and P. G. Schulam, "Flexible ureteroscopy and laser lithotripsy for multiple unilateral intrarenal stones," *Eur. Urol.*, vol. 55, no. 5, pp. 1190–1197, 2009.
[11] R. Saglam, A. Y. Muslumanoglu, Z. Tokatlı, T. Çaşkurlu, K. Sarica, A. I. Taşçi, B. Erkurt, E. Süer, A. S. Kabakci, and G. Preminger, "A new robot for flexible ureteroscopy: Development and early clinical results (ideal stage 1–2b)," *Eur. Urol.*, vol. 66, no. 6, pp. 1092–1100, 2014.
[12] B. Geavlete, R. Saglam, D. Georgescu, R. Multescu, V. Iordache, A. Kabakci, C. Ene, and P. Geavlete, "The importance of the ergonomy in robotic flexible ureteroscopy versus standard flexible ureteroscopy," *Eur. Urol. Suppl.*, vol. 15, no. 11, p. e1454, 2016.
[13] *Virtual Reality Training Platform for Flexible Ureterorenoscopy Interventions With a Minimally Invasive Surgical Robot*, Universidad del País Vasco, Leioa, Spain, 2017.
[14] M. Müller, B. Heidelberger, M. Hennix, and J. Ratcliff, "Position based dynamics," *J. Vis. Commun. Image Represent.*, vol. 18, no. 2, pp. 109–118, 2007.
[15] M. Müller, B. Heidelberger, M. Teschner, and M. Gross, "Meshless deformations based on shape matching," *ACM Trans. Graph.*, vol. 24, no. 3, pp. 471–478, 2005.
[16] B. Jaffray, "Minimally invasive surgery," *Arch. Disease Childhood*, vol. 90, no. 5, pp. 537–542, 2005.
[17] M. J. Mack, "Minimally invasive and robotic surgery," *Jama*, vol. 285, no. 5, pp. 568–572, 2001.
[18] B. M. Smithers, D. C. Gotley, I. Martin, and J. M. Thomas, "Comparison of the outcomes between open and minimally invasive esophagectomy," *Ann. Surg.*, vol. 245, no. 2, p. 232, 2007.
[19] A. M. Lacy, S. Delgado, A. Castells, H. A. Prins, V. Arroyo, A. Ibarzabal, and J. M. Pique, "The long-term results of a randomized clinical trial of laparoscopy-assisted versus open surgery for colon cancer," *Ann. Surg.*, vol. 248, no. 1, pp. 1–7, 2008.
[20] J. Guillotreau, X. Gamé, M. Mouzin, N. Doumerc, R. Mallet, F. Sallusto, B. Malavaud, and P. Rischmann, "Radical cystectomy for bladder cancer: Morbidity of laparoscopic versus open surgery," *J. Urol.*, vol. 181, no. 2, pp. 554–559, 2009.
[21] K. Fuchs, "Minimally invasive surgery," *Endoscopy*, vol. 34, no. 2, pp. 154–159, 2002.
[22] A. Park, G. Lee, F. J. Seagull, N. Meenaghan, and D. Dexter, "Patients benefit while surgeons suffer: An impending epidemic," *J. Amer. College Surgeons*, vol. 210, no. 3, pp. 306–313, 2010.
[23] K. Miller, M. Benden, A. Pickens, E. Shipp, and Q. Zheng, "Ergonomics principles associated with laparoscopic surgeon injury/illness," *Hum. Factors*, vol. 54, no. 6, pp. 1087–1092, 2012.
[24] P. P. Rao, "Robotic surgery: New robots and finally some real competition!" *World J. Urol.*, vol. 36, no. 4, pp. 537–541, 2018.
[25] M. Runciman, A. Darzi, and G. Mylonas, "Soft robotics in minimally invasive surgery," *Soft Robot.*, vol. 6, no. 4, pp. 423–443, 2019.
[26] E. Lee, A. Rafiq, R. Merrell, R. Ackerman, and J. Dennerlein, "Ergonomics and human factors in endoscopic surgery: A comparison of manual vs telerobotic simulation systems," *Surgical Endoscopy Interventional Techn.*, vol. 19, no. 8, pp. 1064–1070, 2005.
[27] X. Ma, C. Song, P. W. Chiu, and Z. Li, "Autonomous flexible endoscope for minimally invasive surgery with enhanced safety," *IEEE Robot. Autom. Lett.*, vol. 4, no. 3, pp. 2607–2613, Jul. 2019.
[28] G.-B. Cadiere, J. Himpens, O. Germay, R. Izizaw, M. Degueldre, J. Vandromme, E. Capelluto, and J. Bruyns, "Feasibility of robotic laparoscopic surgery: 146 cases," *World J. Surg.*, vol. 25, no. 11, pp. 1467–1477, 2001.
[29] A. Pigazzi, J. Ellenhorn, G. Ballantyne, and I. Paz, "Robotic-assisted laparoscopic low anterior resection with total mesorectal excision for rectal cancer," *Surgical Endoscopy Interventional Techn.*, vol. 20, no. 10, pp. 1521–1525, 2006.
[30] P. J. Coronado, M. A. Herraiz, J. F. Magrina, M. Fasero, and J. A. Vidart, "Comparison of perioperative outcomes and cost of robotic-assisted laparoscopy, laparoscopy and laparotomy for endometrial cancer," *Eur. J. Obstetrics Gynecol. Reproductive Biol.*, vol. 165, no. 2, pp. 289–294, 2012.
[31] G. Hubens, H. Coveliers, L. Balliu, M. Ruppert, and W. Vaneerdeweg, "A performance study comparing manual and robotically assisted laparoscopic surgery using the da vinci system," *Surgical Endoscopy Interventional Techn.*, vol. 17, no. 10, pp. 1595–1599, 2003.
[32] S. Maeso, M. Reza, J. A. Mayol, J. A. Blasco, M. Guerra, E. Andradas, and M. N. Plana, "Efficacy of the da vinci surgical system in abdominal surgery compared with that of laparoscopy: A systematic review and meta-analysis," *Ann. Surg.*, vol. 252, no. 2, pp. 254–262, 2010.
[33] S. G. Alletti, C. Rossitto, F. Fanfani, A. Fagotti, B. Costantini, S. Gidaro, G. Monterossi, L. Selvaggi, and G. Scambia, "Telelap ALF-X–assisted laparoscopy for ovarian cyst enucleation: Report of the first 10 cases," *J. Minimally Invasive Gynecol.*, vol. 22, no. 6, pp. 1079–1083, 2015.
[34] F. Fanfani, S. Restaino, S. G. Alletti, A. Fagotti, G. Monterossi, C. Rossitto, B. Costantini, and G. Scambia, "Telelap ALF–x robotic-assisted laparoscopic hysterectomy: Feasibility and perioperative outcomes," *J. Minimally Invasive Gynecol.*, vol. 22, no. 6, pp. 1011–1017, 2015.
[35] F. Fanfani, G. Monterossi, A. Fagotti, C. Rossitto, S. G. Alletti, B. Costantini, V. Gallotta, L. Selvaggi, S. Restaino, and G. Scambia, "The new robotic telelap ALF-x in gynecological surgery: Single-center experience," *Surgical Endoscopy*, vol. 30, no. 1, pp. 215–221, 2016.
[36] M. J. Lum, D. C. Friedman, G. Sankaranarayanan, H. King, K. Fodero, R. Leuschke, B. Hannaford, J. Rosen, and M. N. Sinanan, "The raven: Design and validation of a telesurgery system," *Int. J. Robot. Res.*, vol. 28, no. 9, pp. 1183–1197, 2009.
[37] J. A. Cadeddu, D. Stoianovici, R. N. Chen, R. G. Moore, and L. R. Kavoussi, "Stereotactic mechanical percutaneous renal access," *J. Endourol.*, vol. 12, no. 2, pp. 121–125, 1998.
[38] L.-M. Su, D. Stoianovici, T. W. Jarrett, A. Patriciu, W. W. Roberts, J. A. Cadeddu, S. Ramakumar, S. B. Solomon, and L. R. Kavoussi, "Robotic percutaneous access to the kidney: Comparison with standard manual access," *J. Endourol.*, vol. 16, no. 7, pp. 471–475, 2002.
[39] S. Ernst, F. Ouyang, C. Linder, K. Hertting, F. Stahl, J. Chun, H. Hachiya, D. Bänsch, M. Antz, and K.-H. Kuck, "Initial experience with remote catheter ablation using a novel magnetic navigation system: Magnetic remote catheter ablation," *Circulation*, vol. 109, no. 12, pp. 1472–1475, 2004.
[40] F. Kiemeneij, M. S. Patterson, G. Amoroso, G. Laarman, and T. Slagboom, "Use of the stereotaxis niobe magnetic navigation system for percutaneous coronary intervention: Results from 350 consecutive patients," *Catheterization Cardiovascular Intervent.*, vol. 71, no. 4, pp. 510–516, 2008.
[41] M. M. Desai, M. Aron, I. S. Gill, G. Pascal-Haber, O. Ukimura, J. H. Kaouk, G. Stahler, F. Barbagli, C. Carlson, and F. Moll, "Flexible robotic retrograde renoscopy: Description of novel robotic device and preliminary laboratory experience," *Urology*, vol. 72, no. 1, pp. 42–46, 2008.
[42] M. M. Desai, R. Grover, M. Aron, A. Ganpule, S. S. Joshi, M. R. Desai, and I. S. Gill, "Robotic flexible ureteroscopy for renal calculi: Initial clinical experience," *J. Urol.*, vol. 186, no. 2, pp. 563–568, 2011.
[43] P. Geavlete, R. Saglam, D. Georgescu, R. Multescu, V. Iordache, A. S. Kabakci, C. Ene, and B. Geavlete, "Robotic flexible ureteroscopy versus classic flexible ureteroscopy in renal stones: The initial romanian experience," *Chirurgia*, vol. 111, no. 4, pp. 326–329, 2016.
[44] A. Navaratnam, H. Abdul-Muhsin, and M. Humphreys, "Updates in urologic robot assisted surgery," *F1000 Res.*, vol. 7, no. 1, 2018, Art. no. 15480.1.
[45] K. Kunkler, "The role of medical simulation: An overview," *Int. J. Med. Robot. Comput. Assist. Surg.*, vol. 2, no. 3, pp. 203–210, 2006.
[46] R. Al Bareeq, S. Jayaraman, B. Kiaii, C. Schlachta, J. D. Denstedt, and S. E. Pautler, "The role of surgical simulation and the learning curve in robot-assisted surgery," *J. Robotic Surg.*, vol. 2, no. 1, pp. 11–15, 2008.
[47] C. Våpenstad and S. N. Buzink, "Procedural virtual reality simulation in minimally invasive surgery," *Surgical Endoscopy*, vol. 27, no. 2, pp. 364–377, 2013.
[48] M. S. Michel, T. Knoll, K. U. Köhrmann, and P. Alken, "The uro mentor: Development and evaluation of a new computer-based interactive training system for virtual life-like simulation of diagnostic and therapeutic endourological procedures," *BJU Int.*, vol. 89, no. 3, pp. 174–177, 2002.

[49] T. Inoue, S. Okada, S. Hamamoto, and T. Matsuda, "New advanced bench model for flexible ureteroscopic training: The smart simulator," *J. Endourol.*, vol. 32, no. 1, pp. 1–11, 2018.
[50] J. D. Watterson and J. D. Denstedt, "Ureteroscopy and cystoscopy simulation in urology," *J. Endourol.*, vol. 21, no. 3, pp. 263–269, 2007.
[51] M. A. White, A. P. DeHaan, D. D. Stephens, A. A. Maes, and T. J. Maatman, "Validation of a high fidelity adult ureteroscopy and renoscopy simulator," *J. Urol.*, vol. 183, no. 2, pp. 673–677, 2010.
[52] L. Zhang, R. Khare, E. Wilson, S. Wang, C. A. Peters, and K. Cleary, "Robotic assistance for manipulating a flexible endoscope," in *Proc. IEEE Int. Conf. Robot. Autom. (ICRA)*, May/Jun. 2014, pp. 5380–5385.
[53] (2019). *CHAI3D*. Accessed: Aug. 2019. [Online]. Available: http://www.chai3d.org/
[54] D. C. Ruspini, K. Kolarov, and O. Khatib, "The haptic display of complex graphical environments," in *Proc. 24th Annu. Conf. Comput. Graph. Interact. Techn.* Reading, MA, USA: Addison-Wesley, 1997, pp. 345–352.

MARÍA PERAL-BOIZA received the B.S. degree and the M.S. degree in telecommunication engineering from the Universidad Politécnica de Madrid, Spain, in 2016 and 2018, respectively. She is currently a Research Collaborator with the Intelligent Control Laboratory, E.T.S. Ingenieros de Telecomunicación, Universidad Politécnica de Madrid. Her research interest includes haptic systems in surgical and robotic applications.

TERESA GÓMEZ-FERNÁNDEZ was born in Oviedo, Asturias, Spain, in 1994. She received the B.S. and M.S. degrees in telecommunication engineering from the Technical University of Madrid (UPM), in 2018, and the M.S. degree in electrical engineering from the Illinois Institute of Technology, Chicago, in 2018. She was a member of the Electrical Engineering Students' European Association (EESTEC) and the Center for Biomedical Technology (CTB-UPM). Since 2018, she has been working in the software industry in Chicago. She is currently a Research Collaborator with the Intelligent Control Laboratory, Universidad Politécnica de Madrid, Spain. Her research interests include computer-aided detection and diagnosis systems, and telesurgery.

PATRICIA SÁNCHEZ-GONZÁLEZ received the Ph.D. degree in biomedical engineering from the Universidad Politécnica de Madrid. She has teaching experience, since 2007, and a tutoring record of more than 50 grade and master students in their final dissertations. She is currently an Assistant Professor with the E.T.S. Ingenieros de Telecomunicación, Universidad Politécnica de Madrid. She is also the Director of the "Surgical training and image guided surgery" Laboratory, Center for Biomedical Technology. She has published 26 journal articles, 70 congress articles, and three book chapters. Her main research field focuses on the development of new image processing methodologies for diagnosis and quantification of lesions, and solutions for healthcare education, with a special focus in minimally invasive surgery (MIS). In recent years, she has participated in 15 national research projects and ten European research projects.

BORJA RODRÍGUEZ-VILA was born in Madrid, Spain, in 1980. He received the B.S. degree in telecommunications engineering and the Ph.D. degree in biomedical engineering from the Universidad Politécnica de Madrid, Madrid, in 2006 and 2013, respectively. From 2006 to 2017, he was a Researcher with the Group of Telemedicine and Bioengineering, E.T.S. Ingenieros de Telecomunicación, Universidad Politécnica de Madrid. From 2016 to 2018, he was an Assistant Professor with the Universidad Europea de Madrid, Madrid, where he has been a Professor, since 2019. His research interests include image-based surgery, medical image processing, virtual reality, and 3D printing. He is member of the Spanish Society of Biomedical Engineering.

ENRIQUE J. GÓMEZ (S'83–M'85–SM'06) is a Full Professor of biomedical engineering with the Universidad Politécnica de Madrid, Madrid, Spain. He is the Head of the PT and Bioengineering Department, the Director of the Bioengineering and Telemedicine Research Group, UPM, and the Director of the MSc in Biomedical Engineering, UPM. He is also a Senior Researcher with the National Research Center CIBER-BBN, Spanish National Institute of Health (ISCIII). He is currently the President of EIT Health Spain (European Institute for Innovation and Technology in Health). He is the author or coauthor of 177 journal scientific articles and 364 publications in international and national conference proceedings in related fields and has directed 51 national and international research projects. His current research interests include image-guided surgery and neurorehabilitation engineering. He was a founder member of the European Alliance for Medical and Biological Engineering and Science (EAMBES), in 2000, and board society member, from 2005 to 2009. He is an Honorary Life Member, in 2018, of International Federation for Medical and Biological Engineering (IFMBE). Since 2004, he has been the Secretary General of the Spanish Society of Biomedical Engineering (SEIB).

ÁLVARO GUTIÉRREZ (S'99–M'08–SM'12) received the M.Sc. degree in electronic engineering and the Ph.D. degree in computer science from the Universidad Politécnica de Madrid (UPM), Madrid, Spain, in 2004 and 2009, respectively. He was a Visiting Researcher with the Institut de Recherches Interdisciplinaires et de Développements en Intelligence Artificielle, Université Libre de Bruxelles, Brussels, Belgium, in 2008. He is currently an Associate Professor of automatic and control systems with the E.T.S. Ingenieros de Telecomunicación, UPM. He has authored or coauthored three book chapters, and more than 50 refereed journal articles and conference proceeding papers. His research interests include swarm robotics, control systems, sensor networks, haptic systems in surgical, robotic applications, and demand-side management applications, especially focused on smart grids and renewable energies.